Direct bonding diamond to zinc selenide

HENRY G. STENHOUSE,* STEPHEN J. BEECHER, AND JACOB I. MACKENZIE

Optoelectronics Research Centre, University of Southampton, Highfield, Southampton. SO17 1BJ, United Kingdom
hgs1g09@soton.ac.uk

Abstract: We report direct bonding of 5mm⌀ x 500μm thick polycrystalline CVD-grown diamond to 25mm⌀ x 4mm ZnSe via a plasma-assisted technique. In addition, diamond to C-cut sapphire bonding is demonstrated via the same approach. Durability of the diamond/ZnSe bond is tested over a temperature range -40 to 150°C and under various ramp rates, demonstrating strong adhesion over the majority of the bond up to a temperature of 80°C. Optical transmission at a wavelength of 1μm shows near ideal transmission when compared to bare ZnSe. Heatspreading performance of the bonded composite is investigated using a pump-probe arrangement, demonstrating at least two-orders of magnitude reduction in the thermal-lens power compared to ZnSe alone.

OCIS codes: (160.0160) Materials; (160.4670) Optical materials; (140.0140) Lasers and laser optics.

References and links

1. V. G. Savitski, S. Reilly, and A. J. Kemp, "Steady-State Raman Gain in Diamond as a Function of Pump Wavelength," IEEE J. Quantum Electron. **49**(2), 218–223 (2013).
2. R. Mildren and A. Sabella, "Highly efficient diamond Raman laser," Opt. Lett. **34**(18), 218–223 (2013).
3. E. Worner, C. Wild, W. Muller-Sebert, R. Locher, and P. Koidl "Thermal conductivity of CVD diamond films: high-precision, temperature-resolved measurements," Diamond Relat. Mater. **5**(6), 688–692 (1996).
4. I. T. Sorokina, "Cr^{2+}-doped II-VI materials for lasers and nonlinear optics," Opt. Mater. **26**(4), 395–412 (2004).
5. J. R. Macdonald, S. J. Beecher, P. A. Berry, G. Brown, K. L. Schepler, A. K. Kar, "Efficient mid-infrared Cr:ZnSe channel waveguide laser operating at 2486nm," Opt. Lett. **38**(13), 2194–2196 (2013).
6. I. Moskalev, S. Mirov, M. Mirov, S. Vasilyev, V. Smolski, A. Zakrevskiy, and V. Gapontsev "140 W Cr:ZnSe laser system," Opt. Express **24**(18), 21090–21104 (2016).
7. A. M. Zaitsev, *Optical Properties of Diamond: A Data Handbook* (Springer–Verlag, 2001).
8. D. T. F. Marple, "Refractive Index of ZnSe, ZnTe, and CdTe," J. Appl. Phys., **35**(3), 539–542 (1964).
9. J. I. Mackenzie, "Dielectric Solid-State Planar Waveguide Lasers: A Review," IEEE J. Sel. Topics Quantum Electron., **13**(3), 626–637 (2007).
10. K. L. Schepler, R. D. Peterson, P. A. Berry, and J. B. McKay, "Thermal effects in Cr^{2+}:ZnSe thin disk lasers," IEEE J. Sel. Topics Quantum Electron. **11**(3), 713–720 (2005).
11. I. Shoji, Y. Okuyama, H. Ichikawa, Y. Ariga, and T. Onda, "Laser Characteristics of Nd:YAG/diamond and Nd:YVO4/diamond Composite Devices Fabricated with the Room-temperature-bonding Technique," in *Advanced Solid State Lasers*, OSA Technical Digest Series (Optical Society of America, 2015) paper ATh2A.14.
12. J. Liang, S. Masuya, M. Kasu, and N. Shigekawa, "Realization of direct bonding of single crystal diamond and Si substrates," Appl. Phys. Lett. **110**(11), 111603 (2017)
13. H. Lee, H. E. Meissner, and O. R. Meissner, "Adhesive-free-bond (AFB) CVD diamond/sapphire and CVD diamond/YAG crystal composites," Proc. SPIE **6216**, (2006).
14. C. Rothhardt, M. Rekas, G. Kalkowski, R. Eberhardt, and A. Tunnermann, "New approach to fabrication of a Faraday isolator for high power laser applications," Fiber Lasers IX: Technology, Systems, and Applications **8237**, (2012).
15. D. J. Pickrell, K. A. Kline, and R. E. Taylor, "Thermal expansion of polycrystalline diamond produced by chemical vapor deposition," Appl. Phys. Lett. **64**(18), 2353–2355 (1994).
16. C–H. Su, S. Feth, and S. L. Lehoczky, "Thermal expansion coefficient of ZnSe crystal between 17 and 1080°C by interferometry," Mater. Lett. **63**(17), 1475–1477 (2009).

1. Introduction

Diamond is proving an increasingly important material in optical and electronic devices due to its excellent non-linear (Raman) [1, 2], mechanical and thermal properties. Diamond's unrivalled thermal conductivity (>1500$Wm^{-1}K^{-1}$@300K) [3] is over 50 times greater than that of sapphire (27$Wm^{-1}K^{-1}$) [4] , making it an ideal material for heatspreading. In addition, diamond's hardness

renders it extremely resistant to wear or indentation damage, offering an appealing structural support for more fragile materials. Zinc selenide (ZnSe) has been demonstrated as an excellent host medium for use in mid-infrared laser operation when doped with chromium or iron [5]. Recent advances have pushed laser output powers to 140W in a disk architecture, but significant efforts are required to mitigate the strong thermal lensing effects [6] that arise from ZnSe's high thermo-optical coefficient ($\frac{dn}{dT}$) of $70 \times 10^{-6}\mathrm{K}^{-1}$ [4]. In contrast to diamond, ZnSe suffers from an extremely low mechanical hardness (Knoop 120, compared with diamond's Knoop 5,700-10,400) and has significantly lower thermal conductivity ($18\mathrm{Wm}^{-1}\mathrm{K}^{-1}$@298K) [4]. Combination of the two materials is therefore of interest for engineered media, allowing diamond to compliment ZnSe's optical properties through both thermal and mechanical protection. Moreover, the refractive indices of diamond and zinc selenide (2.394 and 2.503 at 1µm, respectively) [7,8] make waveguide structures an appealing prospect. A ZnSe/diamond waveguide could be constructed with a relatively high numerical aperture and a pump-guiding structure with excellent mode selection capabilities [9]. Critically, for example, a Cr:ZnSe waveguide laser with a pump wavelength around 2µm and emission between 2-3µm, can be conceived where a diamond cladding could act to provide additional loss for higher-order modes, leading to improved mode selection designs for mid-IR operation. For power-scaling Cr:ZnSe mid-IR lasers, the thin-disk architecture is another promising approach [10], where the heatspreading potential of diamond would provide exceptional performance. However, the mid-infrared absorption of diamond would frustrate operation in the case that the diamond were intra-cavity. As such, the design would require a high-reflectance mirror between the thin-disk and heat spreading diamond layer. While this is the typical design methodology for traditional Yb-doped thin-disk lasers, direct bonding of diamond to a suitable terminating layer (such as Al_2O_3) in the mirror coating would be required. Combining diamond and ZnSe presents difficulties due to the notable difference in Coefficients of Thermal Expansion (CTE), which limit elevated temperature procedures. Direct bonding has proven a versatile approach, demonstrating success in bonding of diamond to dissimilar materials [11–13]. In this work, joining of diamond to ZnSe is achieved at room temperature, using a plasma-assisted direct bond to produce a void-free, optically lossless and thermally conductive interface. To demonstrate the bond's potential for heatspreading in an active waveguide, durability over a range of temperatures and ramp rates was investigated. Localized heating, via an optical pumping scheme, demonstrated that for composite ZnSe/diamond, the thermal lens strength was diminished by several orders of magnitude compared to the bare substrate alone.

2. Direct bonding

2.1. Surface quality

Direct bonding relies on intimate contact between surfaces. In most cases, a nanometer-scale separation must be achieved in order to facilitate successful bonding, requiring stringent polishing and cleaning routines. Desired surface requirements for successful bonding typically include a root mean square (RMS) roughness of <1nm and a flatness of $<\lambda/10$ (@633nm) across the area of interest. Diamond, ZnSe and sapphire faces to be bonded were inspected prior to bonding using a white light interferometer at 5x- (effective 2.5x) and 50x+ (effective 100x) magnifications.

Supplied ZnSe and sapphire were flat to $<\lambda/10$, while diamond was polished to $\sim\lambda/5$. Fig. 1 shows 2D surface maps of each material under 100x magnification, including their S_q, the RMS roughness recorded for each. Diamond was inspected and bonded on the growth side, where the grain size is nominally 1/5th of the thickness and the surface S_q was lower. Fortunately, diamond's poorer surface quality is counteracted by a greater Hamaker constant [13], increasing the van der Waals force produced during bonding. Therefore, provided the appropriate activation, the diamond surface quality was found suitable for bonding.

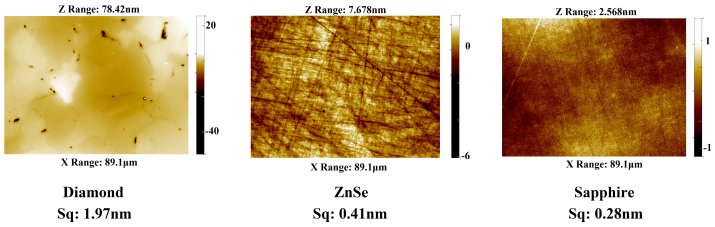

Fig. 1. Surface maps for diamond, ZnSe and sapphire, where S_q is the RMS roughness at 100x magnification.

2.2. Activation and bonding

Plasma-assisted direct bonding demands strict cleanliness of faces. Cleaning, activation and bonding were conducted in a class 1000 clean room environment. Before bonding, all samples were cleaned through a multi-stage, ultrasonic treatment in acetone, isopropanol and de-ionised (DI) water. This serves to agitate and remove organic contaminants from the surface. Following this, the surfaces to be bonded were each activated using a two-stage oxygen and nitrogen plasma clean. The plasma activation provides two benefits: an additional cleaning stage, removing any remaining organic contaminants, and also developing a hydrophilic surface state. Following an acetone wipe, diamond and ZnSe demonstrated measured contact angles of 40° and 70°, respectively. Post plasma activation, both were reduced to <5°, which increased to ~11° after 1hr in atmosphere. Fig. 2 shows water droplets deposited on ZnSe with and without plasma activation. Contact was made within 10 minutes of treatment to reduce the chance of contamination.

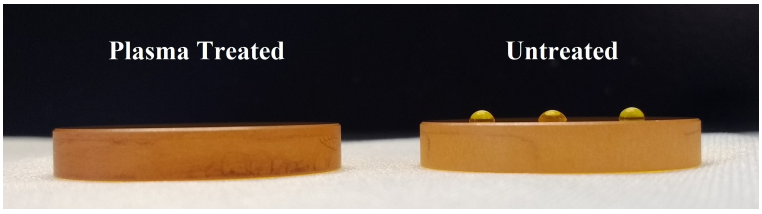

Fig. 2. Water droplets placed on plasma-treated and untreated ZnSe. The activated surface becomes strongly hydrophilic.

Nitrogen plasma has been demonstrated [14] to encourage a hydrophilic state by bombarding the surface, leaving dangling bonds of high surface energy. Following activation, bonding faces were brought together via DI water at room temperature and spontaneously contacted. DI water saturates the surfaces with OH bonds, then capillary forces draw the faces together as it evaporates, bringing them into the short-range regime of hydrogen and van der Waals forces. Bonded samples were then left under a 2.5kg weight for at least 24 hours. Fig. 3 shows the bonded ZnSe and diamond sample. Inspection revealed a clear interface with two small voids visible toward the edge of the bond. The bonding process was confirmed by successfully conducting several further diamond to ZnSe bonds in the same manner.

In addition to the diamond to ZnSe composite, diamond to sapphire bonding was conducted using a similar approach. A diced segment of a 0.67µm-thick sapphire wafer was used as a substrate material. Successful contact was achieved over half of the bond area, displaying a clear interface.

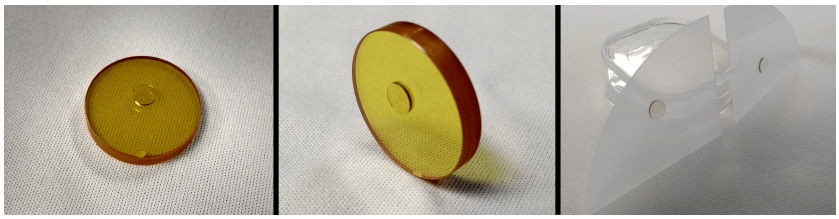

Fig. 3. 500µm thick diamond bonded to 4mm thick ZnSe and 660µm thick sapphire wafers.

3. Temperature trials

Difference in CTE can cause severe stress between bonded materials. Diamond and ZnSe have vastly different CTEs of $1x10^{-6}$/°C (at 300K) [15] and $6.8x10^{-6}$/°C (at 283K) [16], respectively. As such, the bond is unsuitable for the high-temperatures seen in other direct bonding methods [14].

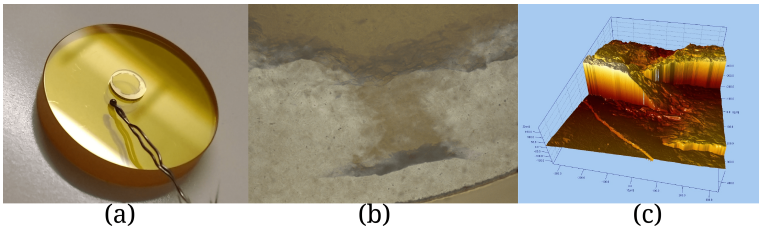

Fig. 4. (a) The diamond/ZnSe composite at 80°C, (b) a 10x microscope inspection of the failed bond region and (c) A 3D surface map of the ZnSe surface following debonding.

A series of trials were conducted to test the composite's resistance to temperature change and ramp rates. The composite was first heated to 80°C in 5°C increments, inspecting at each step. The temperature was measured by a thermocouple close to the diamond on the ZnSe surface. No change was observed up to 55°C, at which the bond area shrank slightly from the edges. By 80°C an unbonded ring was clearly visible around the central bond, as shown in Fig. 4(a). Sharp, dark-lined edges developed around the remaining bonded area, forming a hard barrier to the bond edge. These were inspected using a microscope and (following bond failure) a white light interferometer, and noted as locations where the ZnSe surface had warped, distorting the bulk substrate to maintain contact with the diamond, as shown in Fig. 4(b) and (c). The composite was then held at 80°C for eight hours to test durability. No further degradation was noted. Cooling to room temperature also saw no change to the bonded region, beyond softening of the sharp bond edge lines. Further increase of temperature to 150°C saw the loss of all clarity in the bond. Failure then occurred during cleaning with acetone at room temperature.

A second diamond/ZnSe composite was subjected to rapid changes in the 20-80°C range using a Rapid Thermal Annealer (RTA). The bonded sample was ramped from room temperature to 80°C at rates of 1, 2, 5 and 10°C/minute. As before, heating to 80°C caused the bond region to shrink at the outer edges. However, no further damage was observed at the bonding interface due to increases in ramp rate, demonstrating the bond is resistant to sharp changes in environmental temperature. Afterwards, the bond was then cooled by resting over a liquid nitrogen bath on a metal frame. A nitrogen flow was maintained over the sample to stop condensation forming and restrict the rate of cooling. A minimum temperature of -40°C was recorded when cooling the sample rapidly. The bond was held between -20 and -15°C for 10 minutes. The bond was observed to have suffered minor degradation around the edges of the bonded region, as shown in Fig. 5. This behaviour mirrors the degradation witnessed with increasing temperature, with the

exception of developing hard edges to the bonded region.

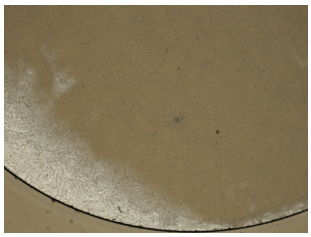

Fig. 5. Microscope inspection of the bond at 5x magnification following cooling to -40°C. Shrinking of the bonded region is noted along the edges.

4. Optical inspection

Distortions caused by the bond interface were inspected using a simple interferometer setup shown in Fig. 6(a). The interference pattern was captured with and without the bonded diamond to ZnSe in one beam path. Any air gaps at the bond interface would be expected to distort the shape of the resulting pattern. Fig. 6(b) shows no distortion was visible in the interference fringes.

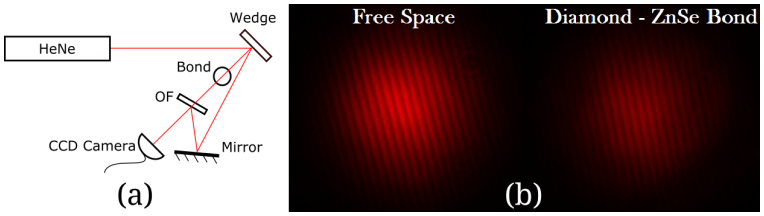

Fig. 6. (a)HeNe interferometer setup for inspecting bond interface optical distortions. One path travels through the bond before recombining with the freespace beam reflected off an Optical Flat (OF). (b) Interference patterns with both beams in free space travel and with one beam passing through the bonded composite.

A 1.064μm laser was then used to record the composite's optical transmission. By using both clear and damaged bonds, it was possible to compare transmission between clear and separated regions. Tab. 1 shows the recorded transmission values. In addition, Fresnel reflections for each material were measured at small angles of incidence (taking care to block subsequent reflections), and theoretical values based on the previously listed refractive index for each material were calculated. The recorded results fall in line with those predicted theoretically, with the exception of the failed bond. In this case, the Fresnel calculation is based on four reflections arising from a contained air gap. However, in reality the failed region contains areas that remain partially bonded, increasing the overall transmission and causing discrepancy in results.

Table 1. Measured and theoretical transmissions at 1.064μm for bare ZnSe, the diamond/ZnSe composite and a region of failed bond.

Region	ZnSe	Clear Bond	Failed Bond
Measured transmission (%)	65.7±1.5	67.4±0.9	54.8±0.9
Calculated transmission from Fresnel reflections (%)	67.5±3.9	68.7±3.4	46.4±3.9
Theoretical transmission based on index (%)	66.6	67.8	46

5. Localised heating trial

To investigate the heat spreading benefits of the bond, a localized heating comparison was conducted between bare ZnSe and bonded diamond/ZnSe. A 445nm diode was collimated by a lens (L1), f=8mm, before focusing by a second lens (L2), f=25mm, to an approximately 30µm x 140µm radius waist near the ZnSe surface. A home-built 1064nm laser was directed through the rear ZnSe face to overlap with the region heated by the 445nm laser on the front surface. The beam was focussed by a lens (L3), f=200mm, to a radius of 140µm. The reflection off this face was captured by a lens (L4), f=150mm, and focused onto a Spiricon CCD positioned at the Fourier plane of the lens, as shown in Fig. 7(a). The absorption coefficient at 445nm was determined to be more than 77cm^{-1}. To maximise the thermal load density, the 445nm beam waist was positioned just within the sample's surface, set for maximum thermal lens.

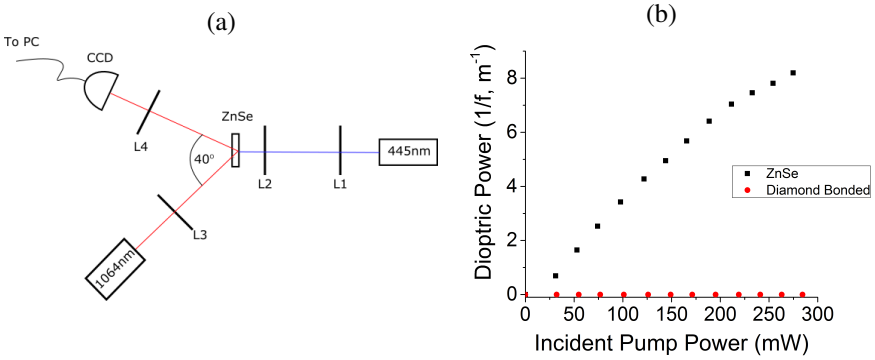

Fig. 7. (a) Pump-probe setup design to compare thermal lensing in bonded and unbonded ZnSe and (b) optical power of induced thermal lens with increasing laser power.

The incident 445nm pump power was raised to 300mW while recording the probe beam diameter. This was repeated in an area covered by the diamond layer. The optical path difference for the diamond was recorded as 720µm at the pump wavelength. The sample was repositioned to find the lowest probe radius before increasing the power. A maximum dioptric power of 8.2m^{-1} was observed for bare ZnSe. Scanned within the bonded region, no thermal lens was detected within our setup's limits. Fig. 7(b) shows the lens' dioptric power recorded in each region.

6. Summary

We have successfully bonded CVD-grown diamond to ZnSe using plasma activation. Despite CTE differences the bond resists -40 to 80°C temperatures. Optical transmission experiments through the bonded region proved that there was an intimate contact between respective surfaces. When compared to bare ZnSe, a localized heating trial demonstrated exceptional heat spreading, reducing the observed thermal lens at least two orders of magnitude in our setup. Several engineered optical structures based on such composites can be envisaged for active and passive devices using this technique. Strength testing of the composite is planned in future experiments.

Funding

Engineering and Physical Sciences Research Council (EPSRC) (EP/J008052/1).

Acknowledgements

H.G. Stenhouse acknowledges support from EPSRC and Gooch & Housego (UK) Ltd. Data presented herein can be found at DOI: 10.5258/SOTON/D0051.